SARS-CoV-2 *ORF3A* interacts with the Clic-like chloride channel-1 (*CLCC1*) and triggers an unfolded protein response

Hannah Gruner [1], **Yaohuan Zhang** [1, 2], **Kaavian Shariati** [1], **Nicholas Yiv** [1], **Zicheng Hu** [1], **Yuhao Wang** [1], **Fielding Hejtmancik** [3], **Michael McManus** [1], **Kevin Tharp** [4], **Gregory Ku** [Corresp. 1, 5]

[1] Diabetes Center, University of California, San Francisco, San Francisco, CA, United States

[2] Metabolic Biology Graduate Program, University of California, Berkeley, Berkeley, CA, United States

[3] National Eye Institute, Bethesda, MD, United States

[4] Center for Bioengineering and Tissue Regeneration, University of California, San Francisco, San Francisco, CA, United States

[5] Division of Endocrinology and Metabolism, University of California, San Francisco, San Francisco, CA, United States

Corresponding Author: Gregory Ku
Email address: gregory.ku@ucsf.edu

Understanding the interactions between SARS-CoV-2 and host cell machinery may reveal new targets to treat COVID-19. We focused on an interaction between the SARS-CoV-2 ORF3A accessory protein and the CLIC-like chloride channel-1 (CLCC1). We found that ORF3A partially co-localized with CLCC1 and that ORF3A and CLCC1 could be co-immunoprecipitated. Since CLCC1 plays a role in the unfolded protein response (UPR), we hypothesized that ORF3A may also play a role in the UPR. Indeed, ORF3A expression triggered a transcriptional UPR that was similar to knockdown of *CLCC1*. ORF3A expression in 293T cells induced cell death and this was rescued by the chemical chaperone taurodeoxycholic acid (TUDCA). Cells with *CLCC1* knockdown were partially protected from ORF3A-mediated cell death. *CLCC1* knockdown upregulated several of the homeostatic UPR targets induced by ORF3A expression, including *HSPA6* and spliced *XBP1,* and these were not further upregulated by ORF3A. Our data suggest a model where *CLCC1* silencing triggers a homeostatic UPR that prevents cell death due to ORF3A expression.

SARS-CoV-2 *ORF3A* interacts with the Clic-like chloride channel-1 (*CLCC1*) and triggers an unfolded protein response

Hannah Gruner[1], Yaohuan Zhang[1,3], Kaavian Shariati[1], Nicholas Yiv[1], Zicheng Hu[4], Yuhao Wang[1], Fielding Hetjmancik[6], Michael T. McManus[1], Kevin Tharp[5], Gregory M. Ku[1,2]

[1]Diabetes Center, University of California San Francisco, San Francisco, CA 94143, USA
[2]Division of Endocrinology and Metabolism, Department of Medicine, University of California San Francisco, San Francisco, CA 94143, USA
[3]Metabolic Biology Graduate Program, University of California Berkeley, Berkeley, CA, USA
[4]Bakar Computational Health Sciences Institute, UCSF, San Francisco, CA 94158, USA
[5]Center for Bioengineering and Tissue Regeneration, Department of Surgery, University of California San Francisco, San Francisco, CA 94143, USA
[6]National Eye Institute, Bethesda, MD, USA

Corresponding Author:
Gregory M. Ku[1,2]
513 Parnassus Ave. HSW 1027, San Francisco, CA 94143, USA
Email address: gregory.ku@ucsf.edu

Abstract

Understanding the interactions between SARS-CoV-2 and host cell machinery may reveal new targets to treat COVID-19. We focused on an interaction between the SARS-CoV-2 ORF3A accessory protein and the CLIC-like chloride channel-1 (CLCC1). We found that ORF3A partially co-localized with CLCC1 and that ORF3A and CLCC1 could be co-immunoprecipitated. Since CLCC1 plays a role in the unfolded protein response (UPR), we hypothesized that ORF3A may also play a role in the UPR. Indeed, ORF3A expression triggered a transcriptional UPR that was similar to knockdown of *CLCC1*. ORF3A expression in 293T cells induced cell death and this was rescued by the chemical chaperone taurodeoxycholic acid (TUDCA). Cells with *CLCC1* knockdown were partially protected from ORF3A-mediated cell death. *CLCC1* knockdown upregulated several of the homeostatic UPR targets induced by ORF3A expression, including *HSPA6* and spliced *XBP1,* and these were not further upregulated by ORF3A. Our data suggest a model where *CLCC1* silencing triggers a homeostatic UPR that prevents cell death due to ORF3A expression.

Introduction

A greater understanding the host-pathogen interactions of SARS-CoV-2, the virus that causes COVID-19, may reveal novel therapeutic targets to reduce the global impact of this disease. While appropriate attention has been paid to the interaction of the spike protein with the ACE2 and TMPRSS2 proteins, the accessory proteins of SARS-CoV-2 are also important for its pathogenesis. SARS-CoV-2 ORF3A is the largest of the accessory proteins, with 275 amino acids encoding a 3-pass transmembrane protein. SARS-CoV-2 ORF3A is 73% identical to SARS-CoV ORF3A, suggesting that insights into SARS-CoV ORF3A may be relevant to the study of SARS-CoV-2 ORF3A. A SARS-CoV virus with a deletion of ORF3A is less cytotoxic without affecting viral replication(Freundt et al. 2010). Expression of SARS-CoV ORF3A alone induces golgi fragmentation(Freundt et al. 2010), the unfolded protein response (UPR) (Minakshi et al. 2009) and NLRP3 inflammasome activation, and cell death(Siu et al. 2019).

Like its counterpart in SARS-CoV, SARS-CoV-2 ORF3A induces cell death(Ren et al. 2020). Point mutations in either the cysteine-rich motif or the YXXΦ motif in SARS-CoV-2 ORF3A reduce membrane localization and reduce its ability to trigger cell death(Ren et al. 2020). Deletion of ORF3A from SARS-CoV-2 substantially reduces its pathogenicity in human ACE2 transgenic mice(Silvas et al. 2021). The cryo-electron microscopy structure of ORF3A reveals a dimeric or tetrameric channel and purified ORF3A in nano disks exhibits non-selective cation channel activity(Kern et al. 2020). SARS-CoV-2 ORF3A interacts with a wide variety of different host proteins and processes(Gordon et al. 2020). SARS-CoV-2 ORF3A-induced cell death is blocked by caspase-8 and caspase-9 inhibitors(Ren et al. 2020). It sequesters VPS39 and prevents autolysosome formation(Miao 2021). ORF3A also localizes to late endosomes; alters endosome morphology(Miserey-Lenkei et al. 2021); and binds to STING to block NF-kB activation(Rui et al. 2021).

High throughput protein interaction studies of SARS-CoV-2 proteins identified the CLIC-like chloride channel-1 (*CLCC1)* as an ORF3A interacting protein(Gordon et al. 2020) and a protein that is differentially phosphorylated upon SARS-CoV-2 infection(Bouhaddou et al. 2020). CLCC1 is a putative chloride channel that localizes predominantly to the endoplasmic reticulum(Nagasawa et al. 2001). A spontaneous mutation disrupting the *Clcc1* gene in mice leads to endoplasmic reticulum (ER) stress and cell death in the cerebellum, resulting in ataxia(Jia et al. 2015). In humans, a point mutation in *CLCC1* causes autosomal recessive retinitis pigmentosa likely due to increased retinal cell death, presumably from increased ER stress(Li et al. 2018).

Given that expression of SARS-CoV ORF3A is sufficient to induce the UPR (Minakshi et al. 2009) and that CLCC1 plays a role in ER stress(Jia et al. 2015; Li et al. 2018), we explored a functional link between *CLCC1* and SARS-CoV-2 *ORF3A.* We confirmed that ORF3A and CLCC1 physically interact. ORF3A expression induced a homeostatic unfolded protein response

as did CLCC1 silencing. Our data suggest that ORF3A triggers the UPR through *CLCC1* and this may play a role in SARS-CoV-2 induced cytotoxicity.

Materials & Methods

Molecular biology:
pDONR207 SARS-CoV-2 ORF3A was a gift from Fritz Roth (Addgene plasmid # 141271; http://n2t.net/addgene:141271 ; RRID:Addgene_141271). An HA tag was added to the 3' end of the open reading frame by PCR and was cloned into pSicoR EF1a, where the EF1a promoter directs expression of ORF3A-HA. The correct sequence was validated by Sanger sequencing. Two guide RNAs to silence human *CLCC1* were cloned into a lentivirus vector expressing from the U6 promoter with GFP and hygromycin resistance. The guide RNA sequences were: GGGAAGCACGCTGAAACCCT and GCCCAGGCCGGCCGCAGAAG. After lentiviral infection of 293T cells stably expressing dCas9KRAB, cells were selected for lentiviral infection using hygromycin (Thermo).

The wild type and human *CLCC1* and D25E mutant *CLCC1* with a N-terminal FLAG tag were subcloned by PCR into a lentiviral expression vector downstream of mCherry-T2A, driven by the CMV promoter. The correct sequence was validated by Sanger sequencing.

Cells:
293T cells stably expressing dCas9KRAB were generated by integration of a donor cassette containing a CMV promoter driving dCas9KRAB with separate EF1a promoter driving puromycin and mCherry flanked by loxP sites. The parental 293T cell was obtained from ATCC. Eight hundred based pair homology arms to the AAVS1 locus flanked the cassettes. The donor DNA was co-transfected with a wild type cDNA and a guide RNA targeting the *AAVS1* genomic locus (GGGGCCACTAGGGACAGGAT)(Mali et al. 2013). Clones were selected using puromycin. Homologous integration was confirmed by genomic DNA PCR. To remove the puromycin and mCherry, 800ng of the Cre plasmid (Addgene plasmid #24971) was transfected and the bulk population was serially diluted to generate single cell clones. Each clone was validated for mCherry loss and puromycin sensitivity and then silencing was validated using silencing of CD146 as a test target.

mRNA-seq:
Total RNA was isolated using an RNeasy Plus Mini kit (Qiagen). PolyA RNA was isolated from one microgram of total RNA (Lexogen) and stranded RNA-seq libraries were prepared (CORALL, Lexogen), indexed and sequenced on a HiSeq 4000 (Illumina) at the UCSF Center for Advanced Technologies. Reads were aligned by HiSat2(Pertea et al. 2016) to the hg38 assembly and gene level counts were made using HTSeq(Anders et al. 2015). The statistical power of this design is 0.75 given a sequencing depth of 4, 3 biological replicates, 0.1 coefficient of variation, to detect a 3-fold difference with an alpha value of 0.05(Hart et al. 2013).

Differential expression analysis were performed with DESeq2(Love et al. 2014). The interaction between CLCC1 and ORF3A were tested with DESeq2 with the following model: Count ~ CLCC1 + ORF3A + CLCC1*ORF3A. GO term enrichment was performed using the Gene Ontology website (release date=2020-07-16)(Ashburner et al. 2000; Mi et al. 2019; The Gene Ontology 2019). Spliced XBP1 mRNA was calculated as a percent of total XBP1 by adding the transcripts per million of ENST00000344347.5+ENST00000611155.4 divided by ENST00000216037.10+ENST00000344347.5+ENST00000611155.4. Significance was determined by ratio ~ CLCC1+ORF3A + CLCC1*ORF3A.

Sequences have been deposited at the NCBI Sequence Read Archive (https://www.ncbi.nlm.nih.gov/sra) under accession number PRJNA887134.

Cell death assay – Flow cytometry

48 hours after transient transfection with plasmids (Jetprime), cells were trypsinized and incubated with Sytox Orange (Thermo) to label dead cells, then analyzed by flow cytometry (Attune, Thermo). Forward and side scatter gates were used to identify for intact cells and the % of cells that were Sytox Orange positive was determined.

Cell death assay – Incucyte

Cells were transiently transfected (Jetprime) with the indicated plasmids into 96 well plates. To reduce cell toxicity, the media was changed 4 hours after transfection and 15 nM final Sytox Green (Thermo) was added to allow detection of dead cells. The % of dead cells was calculated as the number of Sytox Green positive nuclei that overlapped mCherry positive cells divided by the total number of mCherry positive cells. Images were taken 36 hours post-transfection.

Immunoprecipitation

48 hours after transient transfection, cells were lysed in buffer containing 20 mM Tris pH 7.5, 150 mM NaCl, 1% Triton X-100, and 1x cOmplete protease inhibitor cocktail without EDTA (Roche). Lysates were cleared by centrifugation at 21,000xg for 10 minutes and the supernatant was incubated with 1-5 micrograms of antibody pre-bound to 100 uL of protein G Surebeads (Biorad). After tumbling for 2 hours at 4 degrees C, the beads were washed four times with 300 uL of lysis buffer, eluted with 1x LDS sample buffer and western blots were performed.

Antibodies

M2 anti-FLAG (1:100 immunofluorescence, 1:1000 western blot, Sigma F1804), 3F10 anti-HA (1:100 immunofluorescence, 1:3000 western blot, Roche), anti-HA-Tag-488 (1:200, Santa Cruz, sc-7392), anti-GAPDH-hrp (1:10,000 western blot, Sigma, G9525), anti-CLCC1 (1:500, western blot, Proteintech, 26680-1-AP), anti-CLCC1 (1:50, immunofluorescence, Novus Biologicals, NBP1-82793), anti-PDI (1:100 immunofluorescence, Cell Signaling, 45596), anti-PDI (1:100,

Enzo, ADI-SPA-891) conjugated to Alexa Fluor™ 647 with the Alexa Fluor™ 647 Protein Labeling Kit (Thermofisher, A20173), anti-EEA1 (1:100 immunofluorescence, Proteintech, 66218-1-Ig), anti-RCAS1 (1:100, Cell Signaling Technology, 12290), wheat germ agglutinin (Invitrogen, WGA-555 or WGA-488 5.0 µg/mL). Hoechst 33342 (Thermofisher scientific 1:2000).

Microscopy

Cells were grown on Perkin Elmer® CellCarrier-96 ultra tissue culture treated microplates. Growth media was removed and cells were fixed with freshly prepared 4% PFA in PBS for 10 minutes at room temperature and then washed in 1X PBS. Cells were first assessed to confirm transfection success through visualizing mCherry or GFP. Cells were permeabilized and blocked in PBST (1x PBS; 0.1% Triton X-100, 10% FBS) for 90 minutes at room temperature. Fluorophore signal was inactivated using Cyclic Immunofluorescence (PMID: 27925668). Cells were imaged on an Opera Phenix Spinning Disk Confocal (Perkin Elmer). A single optical slice is shown.

Image analysis

ORF3A intensity analysis. Using Harmony image analysis software, segmentation was performed on the nucleus, cell, cytoplasm, membrane for all cells. Cells touching the border were excluded. Within the cell mask, various organelles were segmented depending on the markers used which included ER (PDI), golgi (RCAS1), lysosome (LAMP1), early endosomes (EEA1). The median intensity for anti-HA-ORF3A staining was calculated within the subcellular compartment masks for >1,400 ORF3A transfected cells for each organelle. Within cells, regions with and without ORF3A staining were segmented by using non-transfected control wells to determine thresholds.

Results

A high throughput SARS-CoV-2 protein interaction map identified CLCC1 as an ORF3A interacting protein(Gordon et al. 2020). Confirming these high throughput data, ORF3A immunoprecipitates contained endogenous CLCC1 (**Figure 1A**). Reciprocally, immunoprecipitates of FLAG tagged, wild type CLCC1 contained ORF3A (**Figure 1B**). We also tested the ability of a hypomorphic CLCC1 disease-associated variant with reduced channel activity, CLCC1 D25E(Li et al. 2018), and found this mutation did not affect CLCC1 binding to ORF3A (**Figure 1B**). In cells, endogenous CLCC1 co-localized with the ER as has been previously reported(Li et al. 2018) and a minority of ORF3A-HA (**Figure 1C**). FLAG-CLCC1 or FLAG-CLCC1 D25E again co-localized predominantly with the ER, and with minority of ORF3A-HA (**Figure 1D**). The majority of ORF3A did not colocalize with ER, golgi (**Figure 1E**), plasma membrane (**Figure 1F**), or lysosome (**Figure 1G**) and instead colocalized with the early endosome marker EEA1 (**Figure 1G**). The median intensity of ORF3A staining was highest in the early endosome (**Figure 1H**).

To ask if ORF3A expression results in a transcriptional unfolded protein response (UPR), we examined the global transcriptional response to SARS-CoV-2 ORF3A expression using bulk mRNA-sequencing. ORF3A upregulated 21 genes after multiple testing correction (**Figure 2A and Supplemental Table 1**). Nearly all GO terms enriched in these 21 genes were related the response to unfolded proteins (**Figure 2B**). The most highly upregulated gene (>100 fold) was *HSPA6*, an HSP70 member chaperone classically induced by heat shock, unfolded proteins and dysregulation of HSP90 (Deane & Brown 2018; Kuballa et al. 2015). However, other unfolded protein response (UPR) genes were also upregulated, including *HERPUD1,* a component of the ER associated protein degradation machinery (Belal et al. 2012); *XBP1*, a master regulator of the UPR(Oakes & Papa 2014); *CTH*, the cystathionine gamma-lyase(Maclean et al. 2012); and *ASNS*, asparagine synthetase(Lomelino et al. 2017).

Interleukin 1-beta, which is upregulated by SARS-CoV ORF3A expression in 293T cells(Siu et al. 2019), was not induced by SARS-CoV-2 *ORF3A* expression (no counts in either condition, Supplemental File 1). Only six genes were downregulated after ORF3A expression. Though there was no statistically significant enrichment of any GO term in the downregulated gene list, we noted that *TXNIP*, a pro-apoptotic UPR gene(Lerner et al. 2012; Oslowski et al. 2012), was downregulated by ORF3A expression while the upregulated UPR genes (*HSPA6, HERPUD1, XBP1, CTH, ASNS*) are predicted to increase protein folding capacity. *DDIT3*, another pro-apoptotic UPR gene, was not changed by ORF3A expression (**Supplemental Table 1**). Notably, upregulation of *HSPA6* and downregulation of *TXNIP* has been reported in 293T cells after SARS-CoV-2 infection (Sun et al. 2021).

We then examined gene expression after knockdown of *CLCC1* using CRISPR interference. *CLCC1* knockdown caused upregulation of 9 genes (**Figure 2C and Supplemental Table 2**). Consistent with prior data on *CLCC1*, the upregulated genes were highly enriched for GO terms involving the response to unfolded proteins (**Figure 2D**). Interestingly, as in ORF3A expressing cells, the most highly upregulated gene after *CLCC1* silencing was *HSPA6*, showing a 50-fold increased mRNA expression. *HERPUD1*, upregulated by ORF3A expression, was also upregulated by *CLCC1* silencing. Other UPR genes were upregulated in *CLCC1* silenced cells that were not increased in ORF3A expressing cells, including *DNAJB1*, *HSPA5*, and *HYOU1*. There were only 4 genes that showed downregulation after *CLCC1* silencing (besides *CLCC1* itself) and no GO term was enriched.

Given the similarity between GO term enrichment in the response to ORF3A expression and *CLCC1* knockdown, we compared the global gene expression change induced by *CLCC1* knockdown to the change induced by ORF3A expression and found a modest but significant positive correlation ($R = 0.37$, $p = 2.2e\text{-}16$) (**Figure 2E**). These data show that the transcriptional profile induced by *CLCC1* silencing and *ORF3A* expression are similar and include a homeostatic response to unfolded proteins.

Like SARS-CoV ORF3A (Law et al. 2005), SARS-CoV-2 ORF3A expression induced cell death as has been previously reported (Ren et al. 2020) (**Figure 3A-B)**. SARS-CoV-2 ORF3A induced cell death was blocked by incubation with the chemical chaperone taurodeoxycholic acid (TUDCA) (**Figure 3C-D**), suggesting a that ORF3A induced cell death might involve ER stress.

We then asked if CLCC1 knockdown would impact ORF3A-mediated cell toxicity. Cells with knockdown of *CLCC1* were modestly less susceptible to cell death in response to ORF3A over-expression (**Figure 4A**) despite comparable levels of ORF3A expression (**Figure 4B**). Over-expression of wild type *CLCC1* alone did not induce cell death. However, wild type *CLCC1* over-expression synergized with ORF3A expression to induce cell death. In contrast, over-expression of the D25E mutant allele of *CLCC1* alone caused cell death and this was marginally increased after ORF3A expression (**Figure 4C**). Levels of ORF3A were similar between all conditions of *CLCC1* transfection and control DNA transfection (**Figure 4D**).

Since CLCC1 knockdown activated a homeostatic UPR (upregulating genes such as *HSPA5, HSPA6, HERPUD1, HYOU1, DNAJB1*), we hypothesized that these CLCC1 knockdown cells might be better prepared for the UPR stress of expression of ORF3A. We examined gene expression in *CLCC1*-silenced cells after ORF3A expression and tested for genes regulated by the interaction of *CLCC1* and ORF3A. Two genes were regulated by the interaction of *CLCC1* and ORF3A – *HSPA6* and *HERPUD1* (FDR corrected p values of 8.22e-12 and 8.1e-02 respectively). These genes were upregulated by *CLCC1* knockdown and were only modestly further upregulated after ORF3A expression (**Figure 4E**).

Given the upregulation of *XBP1* by ORF3A expression, we examined the abundance of the spliced form of *XBP1 (sXBP1)* that is generated by activated IRE1. It is this transcript of *XBP1* that encodes a transcription factor that drives the homeostatic UPR (Calfon et al. 2002; Yoshida et al. 2001). There was a statistically significant interaction between *CLCC1* knockdown and ORF3A on *sXBP1* abundance (p=0.04). ORF3A caused an increase in s*XBP1* (p=0.01) in cells with normal *CLCC1* expression, but did not do so in cells that had *CLCC1* knockdown (p=0.87). *CLCC1* knockdown alone caused an increase in spliced XBP1 expression that did not reach statistical significance (p=0.0786) (**Figure 4F**), showing another homeostatic UPR gene that was not further upregulated by ORF3A expression in the setting of *CLCC1* knockdown.

Discussion

Understanding host pathogen interactions for SARS-CoV-2 may lead to new therapeutic opportunities to treat COVID-19. We confirmed high throughput protein interaction data showing that ORF3A physically interacts with the CLCC1, a protein which is required for maintenance of ER homeostasis in retinal cells and in cerebellar granule cells(Jia et al. 2015; Li et al. 2018). Our data show that CLCC1 and ORF3A also *functionally* interact -- the knockdown

or over-expression of CLCC1 impacted ORF3A-induced cell toxicity and the upregulation of UPR genes by ORF3A was weaker in *CLCC1* knockdown cells.

From these data, however, we cannot confidently conclude the molecular mechanism of CLCC1 and ORF3A functional interaction. One model is that ORF3A inactivates CLCC1 through direct or indirect action, leading to ER stress and cell death. However, we do not see increased cell death with *CLCC1* knockdown. Additionally, TUDCA relieves cell death due to ORF3A. Together these data suggest that ORF3A triggers ER stress and cell death independent of CLCC1. Indeed, ORF3A triggers additional pathways independent of ER stress that lead to cell death (e.g. caspase-8 and caspace-9).

We favor the model that ORF3A inactivation of CLCC1 does not increase cell death, but actually triggers a homeostatic UPR. Indeed, terminal UPR genes were not upregulated by CLCC1 knockdown, but homeostatic UPR genes that are predicted to increase folding capacity were (e.g. HSPA6, HERPUD1). In this model, knockdown of CLCC1 might be predicted to reduce ORF3A toxicity by increasing this protective homeostatic UPR response. On the other hand, the over-expression of CLCC1 resulted in increased cell death, which may suggest CLCC1 overexpression might overcome CLCC1 inactivation by ORF3A, preventing this homeostatic UPR normally caused by potential CLCC1 suppression. The over-expression of CLCC1 D25E did not result in increase cell death to the same level as wild type CLCC1 when over-expressed with ORF3A, suggesting that functional CLCC1 is important for the synergy with ORF3A. However, we did note increased cell death with CLCC1 D25E over-expression alone, suggesting that these D25E over-expression experiments be interpreted with caution. Without reciprocal mutations and binding studies, we cannot rule out an effect of CLCC1 over-expression or knockdown that is independent of its binding to ORF3A or even the UPR, especially given the multiple activities of ORF3A. For example, ORF3A inhibits autophagy(Miao 2021), which normally promotes cell survival during chronic ER stress(Ogata et al. 2006). Thus, it is plausible ORF3A overexpression cells are more susceptible to ER stress mediated cell death due to inhibition of the protective autophagy pathway.

ORF3A interacts with many other host proteins besides CLCC1. We suggest that another leading candidate is HMOX1, the heme oxygenase-1, which normally serves to reduce oxidative stress. We found that *HMOX1* mRNA is reduced by ORF3A expression and HMOX1 also physically interacts with ORF3A(Gordon et al. 2020). These data suggest ORF3A interferes with HMOX1 contributions to the oxidative stress response, as others have suggested(Batra et al. 2020).

In contrast to our findings in 293T cells where *CLCC1* silencing did not cause cell death, *CLCC1* depletion in retinal cells and cerebellar cells caused cell death that is presumed to be due to a terminal UPR(Jia et al. 2015; Li et al. 2018). This difference may be because retinal and neuronal cell types are more susceptible to ER stress induced cell death. Therefore, depending on

the cell type infected with SARS-CoV-2, the interaction of ORF3A and CLCC1 may have different outcomes. We also note that ORF3A-HA localized to the EEA1+ early endosome in our studies and not the late endosome as other authors have observed (Miserey-Lenkei et al. 2021). This may be due to the level of over-expression of ORF3A or to differences in the cells used. Our study has other several limitations. Most importantly, we studied ORF3A function in isolation (out of the context of virus infection).

Conclusions

We conclude that SARS-CoV-2 ORF3A activates an UPR and functionally interacts with host *CLCC1*. Modulation of the CLCC1 activity and the UPR might reduce cytotoxicity from ORF3A in the setting of SARS CoV-2 infection.

Acknowledgements

None.

References

Anders S, Pyl PT, and Huber W. 2015. HTSeq--a Python framework to work with high-throughput sequencing data. *Bioinformatics* 31:166-169. 10.1093/bioinformatics/btu638

Ashburner M, Ball CA, Blake JA, Botstein D, Butler H, Cherry JM, Davis AP, Dolinski K, Dwight SS, Eppig JT, Harris MA, Hill DP, Issel-Tarver L, Kasarskis A, Lewis S, Matese JC, Richardson JE, Ringwald M, Rubin GM, and Sherlock G. 2000. Gene ontology: tool for the unification of biology. The Gene Ontology Consortium. *Nat Genet* 25:25-29. 10.1038/75556

Batra N, De Souza C, Batra J, Raetz AG, and Yu AM. 2020. The HMOX1 Pathway as a Promising Target for the Treatment and Prevention of SARS-CoV-2 of 2019 (COVID-19). *Int J Mol Sci* 21. 10.3390/ijms21176412

Belal C, Ameli NJ, El Kommos A, Bezalel S, Al'Khafaji AM, Mughal MR, Mattson MP, Kyriazis GA, Tyrberg B, and Chan SL. 2012. The homocysteine-inducible endoplasmic reticulum (ER) stress protein Herp counteracts mutant alpha-synuclein-induced ER stress via the homeostatic regulation of ER-resident calcium release channel proteins. *Hum Mol Genet* 21:963-977. 10.1093/hmg/ddr502

Bouhaddou M, Memon D, Meyer B, White KM, Rezelj VV, Correa Marrero M, Polacco BJ, Melnyk JE, Ulferts S, Kaake RM, Batra J, Richards AL, Stevenson E, Gordon DE, Rojc A,

Obernier K, Fabius JM, Soucheray M, Miorin L, Moreno E, Koh C, Tran QD, Hardy A, Robinot R, Vallet T, Nilsson-Payant BE, Hernandez-Armenta C, Dunham A, Weigang S, Knerr J, Modak M, Quintero D, Zhou Y, Dugourd A, Valdeolivas A, Patil T, Li Q, Huttenhain R, Cakir M, Muralidharan M, Kim M, Jang G, Tutuncuoglu B, Hiatt J, Guo JZ, Xu J, Bouhaddou S, Mathy CJP, Gaulton A, Manners EJ, Felix E, Shi Y, Goff M, Lim JK, McBride T, O'Neal MC, Cai Y, Chang JCJ, Broadhurst DJ, Klippsten S, De Wit E, Leach AR, Kortemme T, Shoichet B, Ott M, Saez-Rodriguez J, tenOever BR, Mullins RD, Fischer ER, Kochs G, Grosse R, Garcia-Sastre A, Vignuzzi M, Johnson JR, Shokat KM, Swaney DL, Beltrao P, and Krogan NJ. 2020. The Global Phosphorylation Landscape of SARS-CoV-2 Infection. *Cell*. 10.1016/j.cell.2020.06.034

Calfon M, Zeng H, Urano F, Till JH, Hubbard SR, Harding HP, Clark SG, and Ron D. 2002. IRE1 couples endoplasmic reticulum load to secretory capacity by processing the XBP-1 mRNA. *Nature* 415:92-96. 10.1038/415092a

Deane CAS, and Brown IR. 2018. Knockdown of Heat Shock Proteins HSPA6 (Hsp70B') and HSPA1A (Hsp70-1) Sensitizes Differentiated Human Neuronal Cells to Cellular Stress. *Neurochem Res* 43:340-350. 10.1007/s11064-017-2429-z

Freundt EC, Yu L, Goldsmith CS, Welsh S, Cheng A, Yount B, Liu W, Frieman MB, Buchholz UJ, Screaton GR, Lippincott-Schwartz J, Zaki SR, Xu XN, Baric RS, Subbarao K, and Lenardo MJ. 2010. The open reading frame 3a protein of severe acute respiratory syndrome-associated coronavirus promotes membrane rearrangement and cell death. *J Virol* 84:1097-1109. 10.1128/JVI.01662-09

Gordon DE, Jang GM, Bouhaddou M, Xu J, Obernier K, White KM, O'Meara MJ, Rezelj VV, Guo JZ, Swaney DL, Tummino TA, Huettenhain R, Kaake RM, Richards AL, Tutuncuoglu B, Foussard H, Batra J, Haas K, Modak M, Kim M, Haas P, Polacco BJ, Braberg H, Fabius JM, Eckhardt M, Soucheray M, Bennett MJ, Cakir M, McGregor MJ, Li Q, Meyer B, Roesch F, Vallet T, Mac Kain A, Miorin L, Moreno E, Naing ZZC, Zhou Y, Peng S, Shi Y, Zhang Z, Shen W, Kirby IT, Melnyk JE, Chorba JS, Lou K, Dai SA, Barrio-Hernandez I, Memon D, Hernandez-Armenta C, Lyu J, Mathy CJP, Perica T, Pilla KB, Ganesan SJ, Saltzberg DJ, Rakesh R, Liu X, Rosenthal SB, Calviello L, Venkataramanan S, Liboy-Lugo J, Lin Y, Huang XP, Liu Y, Wankowicz SA, Bohn M, Safari M, Ugur FS, Koh C, Savar NS, Tran QD, Shengjuler D, Fletcher SJ, O'Neal MC, Cai Y, Chang JCJ, Broadhurst DJ, Klippsten S, Sharp PP, Wenzell NA, Kuzuoglu D, Wang HY, Trenker R, Young JM, Cavero DA, Hiatt J, Roth TL, Rathore U, Subramanian A, Noack J, Hubert M, Stroud RM, Frankel AD, Rosenberg OS, Verba KA, Agard DA, Ott M, Emerman M, Jura N, von Zastrow M, Verdin E, Ashworth A, Schwartz O, d'Enfert C, Mukherjee S, Jacobson M, Malik HS, Fujimori DG, Ideker T, Craik CS, Floor SN, Fraser JS, Gross JD, Sali A, Roth BL, Ruggero D, Taunton J, Kortemme T, Beltrao P, Vignuzzi M, Garcia-Sastre A, Shokat KM, Shoichet BK, and Krogan NJ. 2020. A SARS-CoV-2 protein interaction map reveals targets for drug repurposing. *Nature*. 10.1038/s41586-020-2286-9

Hart SN, Therneau TM, Zhang Y, Poland GA, and Kocher JP. 2013. Calculating sample size estimates for RNA sequencing data. *J Comput Biol* 20:970-978. 10.1089/cmb.2012.0283

Jia Y, Jucius TJ, Cook SA, and Ackerman SL. 2015. Loss of Clcc1 results in ER stress, misfolded protein accumulation, and neurodegeneration. *J Neurosci* 35:3001-3009. 10.1523/JNEUROSCI.3678-14.2015

Kern DM, Sorum B, Hoel CM, Sridharan S, Remis JP, Toso DB, and Brohawn SG. 2020. Cryo-EM structure of the SARS-CoV-2 3a ion channel in lipid nanodiscs. *bioRxiv*. 10.1101/2020.06.17.156554

Kuballa P, Baumann AL, Mayer K, Bar U, Burtscher H, and Brinkmann U. 2015. Induction of heat shock protein HSPA6 (HSP70B') upon HSP90 inhibition in cancer cell lines. *FEBS Lett* 589:1450-1458. 10.1016/j.febslet.2015.04.053

Law PTW, Wong CH, Au TCC, Chuck CP, Kong SK, Chan PKS, To KF, Lo AWI, Chan JYW, Suen YK, Chan HYE, Fung KP, Waye MMY, Sung JJY, Lo YMD, and Tsui SKW. 2005. The 3a protein of severe acute respiratory syndrome-associated coronavirus induces apoptosis in Vero E6 cells. *J Gen Virol* 86:1921-1930. 10.1099/vir.0.80813-0

Lerner AG, Upton JP, Praveen PV, Ghosh R, Nakagawa Y, Igbaria A, Shen S, Nguyen V, Backes BJ, Heiman M, Heintz N, Greengard P, Hui S, Tang Q, Trusina A, Oakes SA, and Papa FR. 2012. IRE1alpha induces thioredoxin-interacting protein to activate the NLRP3 inflammasome and promote programmed cell death under irremediable ER stress. *Cell Metab* 16:250-264. 10.1016/j.cmet.2012.07.007

Li L, Jiao X, D'Atri I, Ono F, Nelson R, Chan CC, Nakaya N, Ma Z, Ma Y, Cai X, Zhang L, Lin S, Hameed A, Chioza BA, Hardy H, Arno G, Hull S, Khan MI, Fasham J, Harlalka GV, Michaelides M, Moore AT, Coban Akdemir ZH, Jhangiani S, Lupski JR, Cremers FPM, Qamar R, Salman A, Chilton J, Self J, Ayyagari R, Kabir F, Naeem MA, Ali M, Akram J, Sieving PA, Riazuddin S, Baple EL, Riazuddin SA, Crosby AH, and Hejtmancik JF. 2018. Mutation in the intracellular chloride channel CLCC1 associated with autosomal recessive retinitis pigmentosa. *PLoS Genet* 14:e1007504. 10.1371/journal.pgen.1007504

Lomelino CL, Andring JT, McKenna R, and Kilberg MS. 2017. Asparagine synthetase: Function, structure, and role in disease. *J Biol Chem* 292:19952-19958. 10.1074/jbc.R117.819060

Love MI, Huber W, and Anders S. 2014. Moderated estimation of fold change and dispersion for RNA-seq data with DESeq2. *Genome Biol* 15:550. 10.1186/s13059-014-0550-8

Maclean KN, Greiner LS, Evans JR, Sood SK, Lhotak S, Markham NE, Stabler SP, Allen RH, Austin RC, Balasubramaniam V, and Jiang H. 2012. Cystathionine protects against endoplasmic reticulum stress-induced lipid accumulation, tissue injury, and apoptotic cell death. *J Biol Chem* 287:31994-32005. 10.1074/jbc.M112.355172

Mali P, Yang L, Esvelt KM, Aach J, Guell M, DiCarlo JE, Norville JE, and Church GM. 2013. RNA-guided human genome engineering via Cas9. *Science* 339:823-826. 10.1126/science.1232033

Mi H, Muruganujan A, Ebert D, Huang X, and Thomas PD. 2019. PANTHER version 14: more genomes, a new PANTHER GO-slim and improvements in enrichment analysis tools. *Nucleic Acids Res* 47:D419-D426. 10.1093/nar/gky1038

Miao GZ, Hongyu; Li, Yan; Ji, Mingming Ji; Chen, Yong; Shi, Yi,; Bi, Yuhai; Wang, Peihui; Zhang, Hong. 2021. ORF3a of the COVID-19 virus SARS-CoV-2 blocks HOPS complex-mediated assembly of the SNARE complex required for autolysosome formation. *Dev Cell* 56:1-16.

Minakshi R, Padhan K, Rani M, Khan N, Ahmad F, and Jameel S. 2009. The SARS Coronavirus 3a protein causes endoplasmic reticulum stress and induces ligand-independent downregulation of the type 1 interferon receptor. *PLoS One* 4:e8342. 10.1371/journal.pone.0008342

Miserey-Lenkei S, Trajkovic K, D'Ambrosio JM, Patel AJ, Copic A, Mathur P, Schauer K, Goud B, Albanese V, Gautier R, Subra M, Kovacs D, Barelli H, and Antonny B. 2021. A comprehensive library of fluorescent constructs of SARS-CoV-2 proteins and their initial characterization in different cell types. *Biol Cell*. 10.1111/boc.202000158

Nagasawa M, Kanzaki M, Iino Y, Morishita Y, and Kojima I. 2001. Identification of a novel chloride channel expressed in the endoplasmic reticulum, golgi apparatus, and nucleus. *J Biol Chem* 276:20413-20418. 10.1074/jbc.M100366200

Oakes SA, and Papa FR. 2014. The Role of Endoplasmic Reticulum Stress in Human Pathology. *Annu Rev Pathol*. 10.1146/annurev-pathol-012513-104649

Ogata M, Hino S, Saito A, Morikawa K, Kondo S, Kanemoto S, Murakami T, Taniguchi M, Tanii I, Yoshinaga K, Shiosaka S, Hammarback JA, Urano F, and Imaizumi K. 2006. Autophagy is activated for cell survival after endoplasmic reticulum stress. *Mol Cell Biol* 26:9220-9231. 10.1128/MCB.01453-06

Oslowski CM, Hara T, O'Sullivan-Murphy B, Kanekura K, Lu S, Hara M, Ishigaki S, Zhu LJ, Hayashi E, Hui ST, Greiner D, Kaufman RJ, Bortell R, and Urano F. 2012. Thioredoxin-interacting protein mediates ER stress-induced beta cell death through initiation of the inflammasome. *Cell Metab* 16:265-273. 10.1016/j.cmet.2012.07.005

Pertea M, Kim D, Pertea GM, Leek JT, and Salzberg SL. 2016. Transcript-level expression analysis of RNA-seq experiments with HISAT, StringTie and Ballgown. *Nat Protoc* 11:1650-1667. 10.1038/nprot.2016.095

Ren Y, Shu T, Wu D, Mu J, Wang C, Huang M, Han Y, Zhang XY, Zhou W, Qiu Y, and Zhou X. 2020. The ORF3a protein of SARS-CoV-2 induces apoptosis in cells. *Cell Mol Immunol* 17:881-883. 10.1038/s41423-020-0485-9

Rui Y, Su J, Shen S, Hu Y, Huang D, Zheng W, Lou M, Shi Y, Wang M, Chen S, Zhao N, Dong Q, Cai Y, Xu R, Zheng S, and Yu XF. 2021. Unique and complementary suppression of cGAS-STING and RNA sensing- triggered innate immune responses by SARS-CoV-2 proteins. *Signal Transduct Target Ther* 6:123. 10.1038/s41392-021-00515-5

Silvas JA, Vasquez DM, Park JG, Chiem K, Allue-Guardia A, Garcia-Vilanova A, Platt RN, Miorin L, Kehrer T, Cupic A, Gonzalez-Reiche AS, Bakel HV, Garcia-Sastre A, Anderson T, Torrelles JB, Ye C, and Martinez-Sobrido L. 2021. Contribution of SARS-CoV-2 Accessory Proteins to Viral Pathogenicity in K18 Human ACE2 Transgenic Mice. *J Virol* 95:e0040221. 10.1128/JVI.00402-21

Siu KL, Yuen KS, Castano-Rodriguez C, Ye ZW, Yeung ML, Fung SY, Yuan S, Chan CP, Yuen KY, Enjuanes L, and Jin DY. 2019. Severe acute respiratory syndrome coronavirus ORF3a protein activates the NLRP3 inflammasome by promoting TRAF3-dependent ubiquitination of ASC. *FASEB J* 33:8865-8877. 10.1096/fj.201802418R

Sun G, Cui Q, Garcia G, Jr., Wang C, Zhang M, Arumugaswami V, Riggs AD, and Shi Y. 2021. Comparative transcriptomic analysis of SARS-CoV-2 infected cell model systems reveals differential innate immune responses. *Sci Rep* 11:17146. 10.1038/s41598-021-96462-w

The Gene Ontology C. 2019. The Gene Ontology Resource: 20 years and still GOing strong. *Nucleic Acids Res* 47:D330-D338. 10.1093/nar/gky1055

Yoshida H, Matsui T, Yamamoto A, Okada T, and Mori K. 2001. XBP1 mRNA is induced by ATF6 and spliced by IRE1 in response to ER stress to produce a highly active transcription factor. *Cell* 107:881-891. 10.1016/s0092-8674(01)00611-0

489

Figure 1

CLCC1 and ORF3A physically interact.

293T cells were transfected with the indicated plasmids (top). Forty-eight hours after transfection, the cells were lysed and immunoprecipiataion was performed with the indicated antibody. (A) Western blots for CLCC1 and HA are shown for the anti-HA immunoprecipitation. (B) Western blots for HA and FLAG are shown for the anti-FLAG precipitation. Both panels representative of 3 independent experiments. (C) 293T cells transfected with the indicated plasmids were stained for endogenous CLCC1, ORF3A (anti-HA) and the endoplasmic reticulum (anti-PDI). n=2. (D) 293T cells were transfected with wild type CLCC1 of D25E CLCC1 and ORF3A-HA and stained for FLAG, HA, and PDI. n=3. (E) 293T cells were transfected with ORF3A-HA and stained for PDI and RCAS1 (golgi). n=3. (F) 293T cells were transfected with ORF3A-HA and stained for HA and WGA (plasma membrane). n=4 (G) 293T cells were transfected with ORF3A-HA and stained for HA, EEA1, and LAMP1. n=4 (H) For each marker, the median ORF3A intensity in the listed organelle is plotted. Standard deviation is shown. The blue dashed line indicates the median intensity of anti-HA-ORF3A for all ORF3A positive masks, while the red dashed line represents the intensity outside the ORF3A mask within cells. n=4 lysosome, golgi, ER, endo- some, n=8 whole cell, nucleus, membrane, cytoplasm.

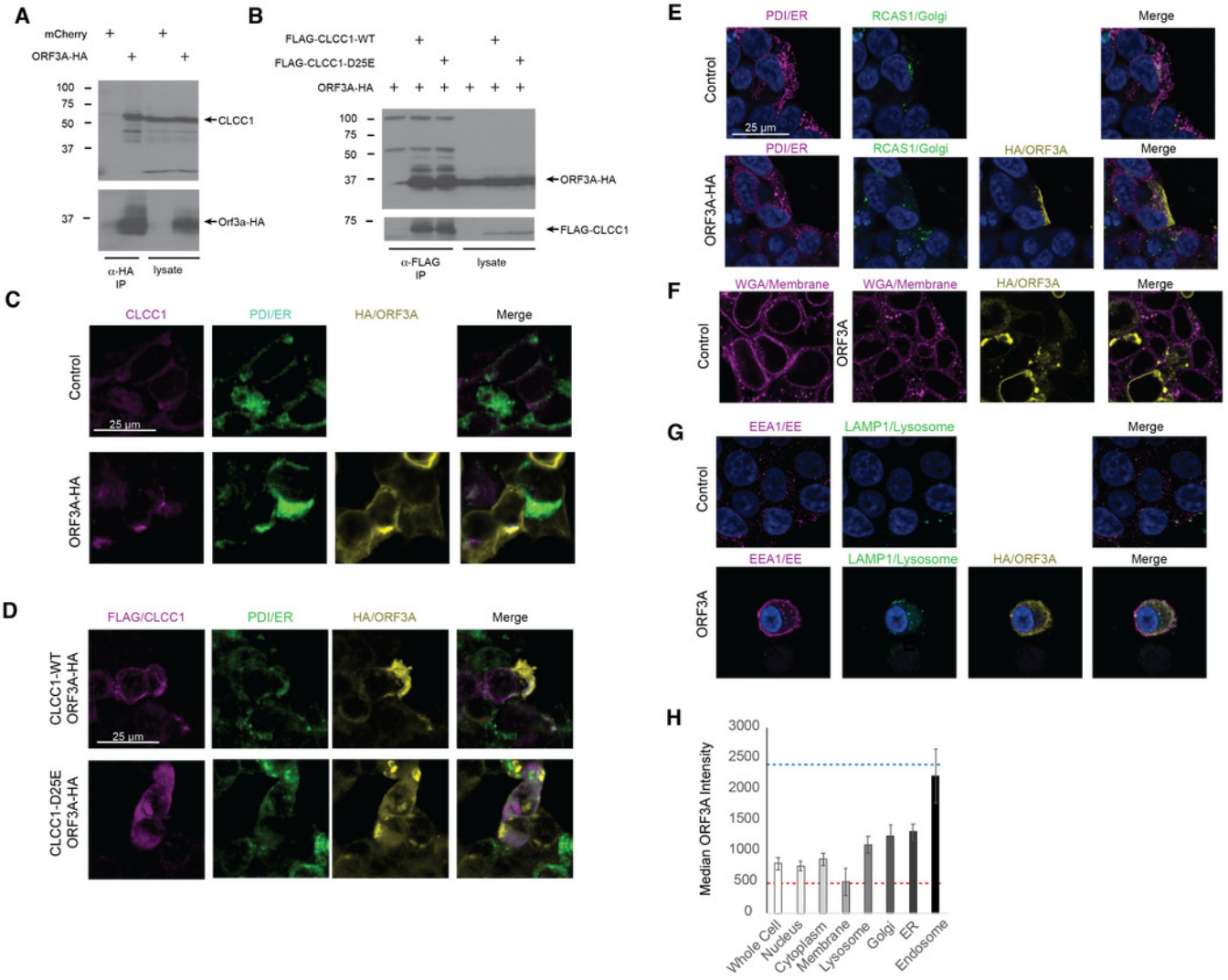
A
mCherry
ORF3A-HA
100
75
50
37
CLCC1
37
Orf3a-HA
α-HA IP
lysate
B
FLAG-CLCC1-WT
FLAG-CLCC1-D25E
ORF3A-HA
100
75
50
37
ORF3A-HA
75
FLAG-CLCC1
α-FLAG IP
lysate
C
CLCC1
PDI/ER
HA/ORF3A
Merge
Control
25 μm
ORF3A-HA
D
FLAG/CLCC1
PDI/ER
HA/ORF3A
Merge
CLCC1-WT ORF3A-HA
25 μm
CLCC1-D25E ORF3A-HA
E
PDI/ER
RCAS1/Golgi
Merge
Control
25 μm
PDI/ER
RCAS1/Golgi
HA/ORF3A
Merge
ORF3A-HA
F
WGA/Membrane
WGA/Membrane
HA/ORF3A
Merge
Control
ORF3A
G
EEA1/EE
LAMP1/Lysosome
Merge
Control
EEA1/EE
LAMP1/Lysosome
HA/ORF3A
Merge
ORF3A
H
Median ORF3A Intensity
3000
2500
2000
1500
1000
500
0
Whole Cell
Nucleus
Cytoplasm
Membrane
Lysosome
Golgi
ER
Endosome

Figure 2

ORF3A expression and CLCC1 silencing both trigger the unfolded protein response.

(A) Volcano plot of gene expression after ORF3A expression compared to control (adjusted p value < 0.05, fold change >1.9 in green). (B) GO terms enriched in genes that are statistically significantly upregulated (adjusted p value <0.05) after ORF3A expression. (C) Volcano plot of gene expression after CLCC1 silencing expression compared to control (adjusted p value < 0.05, fold change >1.9 in green). (D) GO terms enriched in genes that are statistically signifi- cantly upregulated (adjusted p value <0.05) after CLCC1 silencing. (E) Correlation between ORF3A expression and CLCC1 silencing. Each point represents a single gene.

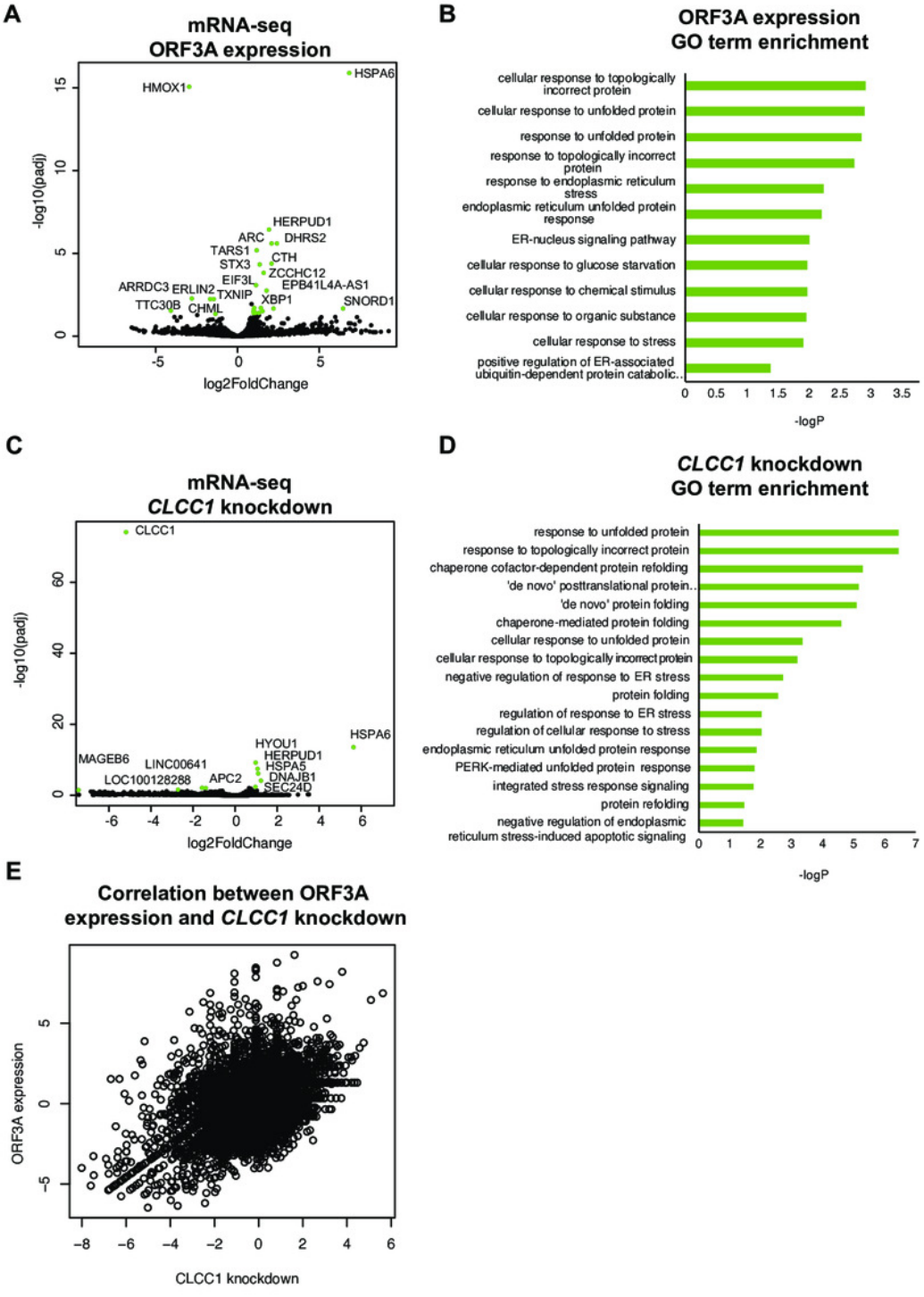
A
mRNA-seq
ORF3A expression
HSPA6
HMOX1
HERPUD1
ARC
DHRS2
TARS1
CTH
STX3
ZCCHC12
EIF3L
EPB41L4A-AS1
ARRDC3
ERLIN2
TXNIP
XBP1
SNORD1
TTC30B
CHML
-log10(padj)
log2FoldChange
B
ORF3A expression
GO term enrichment
cellular response to topologically incorrect protein
cellular response to unfolded protein
response to unfolded protein
response to topologically incorrect protein
response to endoplasmic reticulum stress
endoplasmic reticulum unfolded protein response
ER-nucleus signaling pathway
cellular response to glucose starvation
cellular response to chemical stimulus
cellular response to organic substance
cellular response to stress
positive regulation of ER-associated ubiquitin-dependent protein catabolic..
-logP
C
mRNA-seq
CLCC1 knockdown
CLCC1
HSPA6
HYOU1
HERPUD1
HSPA5
DNAJB1
SEC24D
MAGEB6
LINC00641
LOC100128288
APC2
-log10(padj)
log2FoldChange
D
CLCC1 knockdown
GO term enrichment
response to unfolded protein
response to topologically incorrect protein
chaperone cofactor-dependent protein refolding
'de novo' posttranslational protein..
'de novo' protein folding
chaperone-mediated protein folding
cellular response to unfolded protein
cellular response to topologically incorrect protein
negative regulation of response to ER stress
protein folding
regulation of response to ER stress
regulation of cellular response to stress
endoplasmic reticulum unfolded protein response
PERK-mediated unfolded protein response
integrated stress response signaling
protein refolding
negative regulation of endoplasmic reticulum stress-induced apoptotic signaling
-logP
E
Correlation between ORF3A expression and CLCC1 knockdown
ORF3A expression
CLCC1 knockdown

Figure 3

ORF3A expression induces cell death that is blocked by TUDCA.

(A) 293T cells were transfected with either a vector expressing mCherry or a vector expressing ORF3A-HA. The fraction of cells that were Sytox Green at 48 hours by flow cytometry is plotted. n=6, **p<0.01 by Student's t-test. (B) Cells from A were lysed and a western blot was performed for HA (top) or GAPDH (bottom). (C) As in A, but cells were pre-treated with TUDCA at the indicated concentrations. (D) Cells from C were lysed and a western blot was performed for HA (top) or vinculin (bottom) or CLCC1 (middle).

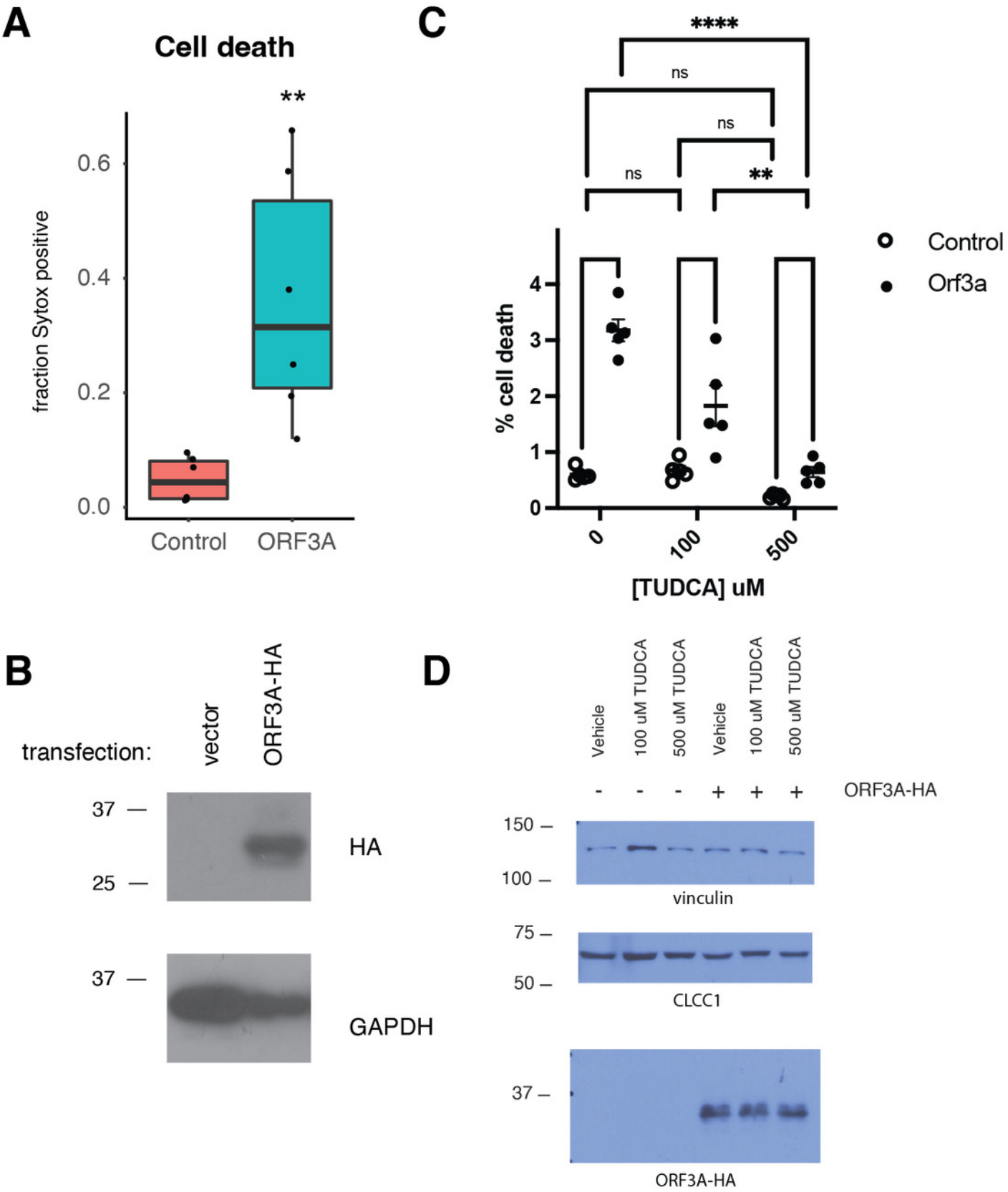
A
Cell death
**
fraction Sytox positive
0.6
0.4
0.2
0.0
Control
ORF3A
C
****
ns
ns
ns
**
% cell death
4
3
2
1
0
0
100
500
[TUDCA] uM
Control
Orf3a
B
transfection:
vector
ORF3A-HA
37
25
HA
37
GAPDH
D
Vehicle
100 uM TUDCA
500 uM TUDCA
Vehicle
100 uM TUDCA
500 uM TUDCA
- - - + + +
ORF3A-HA
150
100
vinculin
75
50
CLCC1
37
ORF3A-HA

Figure 4

CLCC1 functionally interacts with ORF3A.

(A) 293T cells expressing the indicated guide RNAs (top) were transfected with either mCherry or ORF3A-HA. Thirty-six hours after transfection, cell death was normalized to the % cell death observed in non-targeting sgRNA expressing cells with ORF3A expression. n=11. Boxes indicate the median and 75% and 25% percentiles. Two-way ANOVA showed a significant interaction between CLCC1 knockdown and ORF3A over-expression $F(2,48)=25.82$ $p=2.43E-8$. Tukey's HSD post-hoc family wise comparison of means: ****$p<0.0001$. Significance for all comparisons is shown in Supplemental File 3. (B) As in A, but western blots for CLCC1 (top panel), ORF3A-HA (middle panel), and GAPDH (bottom panel). (C) 293T cells were transfect- ed with the indicated plasmids and cell death was measured at 36 hours. n=10 for each condition. Two-way ANOVA showed a significant interaction between ORF3A expression and CLCC1 over-expression: $F(2,54)=31,77$, $p=7.59e-10$. (D) As in D, but western blots were performed for CLCC1 (bottom panel), ORF3A (top panel), and GAPDH (middle panel). (E) Variance stabilizing transformed counts for the indicated genes under the indicated conditions from mRNA-seq. (F) Fraction of spliced XBP1 under indicated conditions.

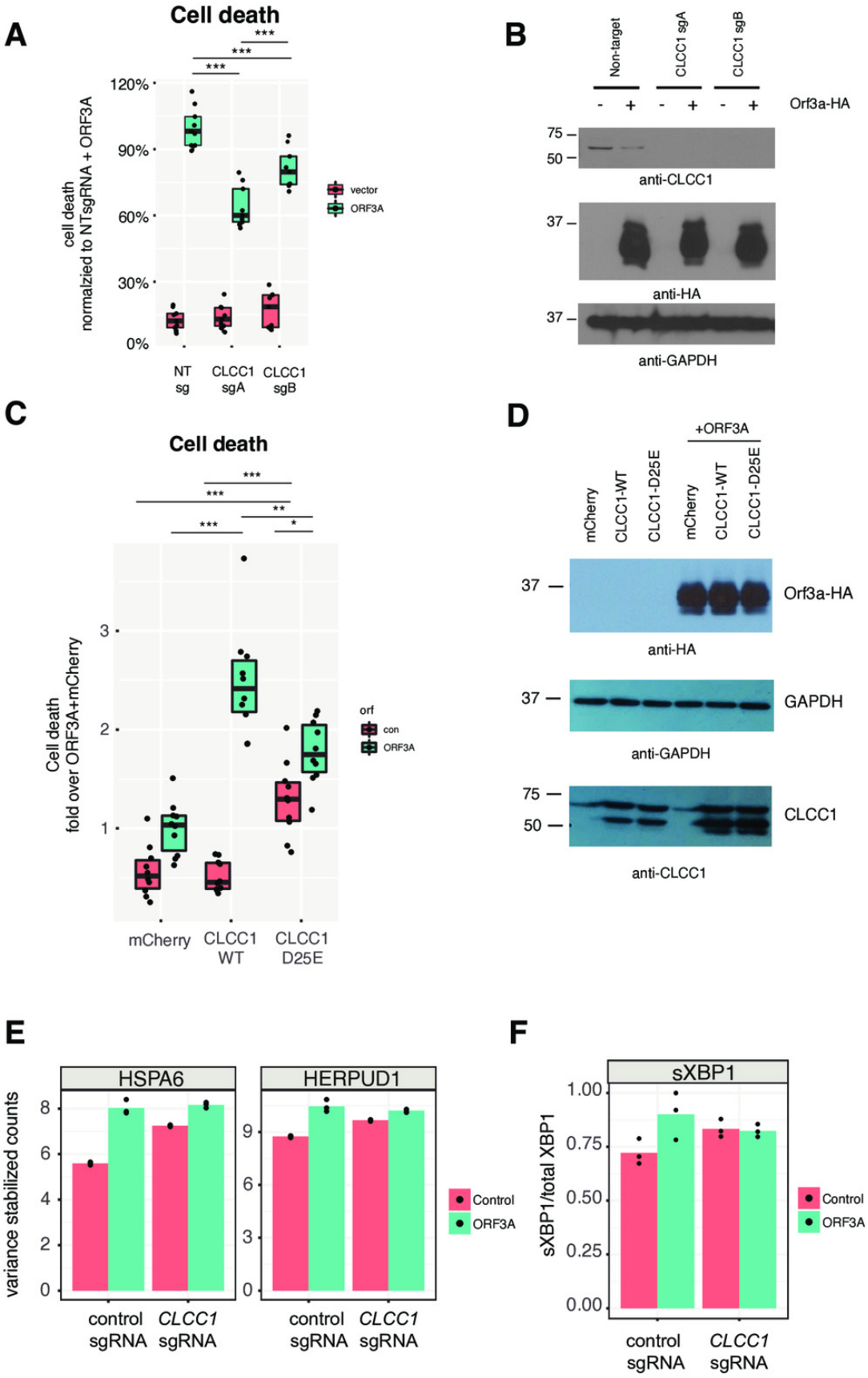
A
Cell death
cell death
normalzied to NTsgRNA + ORF3A
120%
90%
60%
30%
0%
***
***
***
vector
ORF3A
NT sg
CLCC1 sgA
CLCC1 sgB
B
Non-target
CLCC1 sgA
CLCC1 sgB
- + - + - +
Orf3a-HA
75
50
anti-CLCC1
37
anti-HA
37
anti-GAPDH
C
Cell death
Cell death
fold over ORF3A+mCherry
***
***
***
**
*
3
2
1
orf
con
ORF3A
mCherry
CLCC1 WT
CLCC1 D25E
D
+ORF3A
mCherry
CLCC1-WT
CLCC1-D25E
mCherry
CLCC1-WT
CLCC1-D25E
37
Orf3a-HA
anti-HA
37
GAPDH
anti-GAPDH
75
50
CLCC1
anti-CLCC1
E
HSPA6
HERPUD1
variance stabilized counts
8
6
4
2
0
9
6
3
0
Control
ORF3A
control sgRNA
CLCC1 sgRNA
control sgRNA
CLCC1 sgRNA
F
sXBP1
sXBP1/total XBP1
1.00
0.75
0.50
0.25
0.00
Control
ORF3A
control sgRNA
CLCC1 sgRNA